Graphene oxide activates B cells with upregulation of granzyme B expression: evidence at the single-cell level for its immune-modulatory properties and anticancer activity

Marco Orecchioni, Laura Fusco, Raghvendra Mall, Valentina Bordoni, Claudia Fuoco, Darawan Rinchai, Shi Guo, Raquel Sainz, Martina Zoccheddu, Cansu Gurcan, et al.

Graphene oxide activates B cells with upregulation of granzyme B expression: evidence at the single-cell level for its immune-modulatory properties and anticancer activity

Marco Orecchioni,[1]# Laura Fusco,[2,3,4] # Raghvendra Mall,[5]# Valentina Bordoni,[1] Claudia Fuoco,[6] Darawan Rinchai,[2] Shi Guo,[7] Raquel Sainz,[7,§] Martina Zoccheddu,[1] Cansu Gurcan,[8] Acelya Yilmazer,[8] Barbara Zavan,[9] Cécilia Ménard-Moyon,[7] Alberto Bianco,[7] Wouter Hendrickx,[2]* Davide Bedognetti,[2,10]* and Lucia Gemma Delogu[1, 3]*

[1]*Department of Chemistry and Pharmacy University of Sassari, Sassari, Italy;*
[2]*Cancer Research Department, Sidra Medicine, Education City, Doha, Qatar;*
[3]*Department of Biomedical Sciences, University of Padua, Padua, Italy;*
[4]*Department of Chemical and Pharmaceutical Sciences, University of Trieste, Trieste, Italy;*
[5]*Qatar Computing Research Institute (QCRI) Hamad Bin Khalifa University (HBKU), Doha, Qatar.*
[6]*Department of Biology, University of Rome Tor Vergata, Rome, Italy;*
[7]*CNRS, Immunology, Immunopathology and Therapeutic Chemistry, UPR3572, University of Strasbourg, ISIS, 67000 Strasbourg, France;*
[8]*Department of Biomedical Engineering, Faculty of Engineering, Ankara University, Ankara, Turkey;*
[9]*Department of Medical Sciences, University of Ferrara, Ferrara, Italy;*
[10]*Department of Internal Medicine, University of Genova, Genova, Italy*.

*Corresponding authors: luciagemma.delogu@unipd.it; dbedognetti@sidra.org; whendrickx@sidra.org

# These authors contributed equally to this work
§ Current address: Instituto de Catálisis y Petroleoquímica (CSIC) c/ Marie Curie 2, 28049 Madrid, Spain

Keywords

2D materials, nanomedicine, nanotoxicology, single-cell approaches, CyTOF

Abstract

We recently found by single-cell mass cytometry that *ex vivo* human B cells internalize graphene oxide (GO). The functional impact of such uptake on B cells remains unexplored. Here, we disclosed the effects of GO and amino-functionalized GO ($GONH_2$) interacting with human B cells *in vitro* and *ex vivo* at the protein and gene expression levels. Moreover, our study considered three different subpopulations of B cells and their functionality in terms of: i) cytokine production, ii) activation markers, iii) killing activity towards cancer cells. Single-cell mass cytometry screening revealed the higher impact of GO on cell viability towards naïve, memory, and plasma B cell subsets. Different cytokines such as granzyme B (GrB) and activation markers, like CD69, CD80, CD138, and CD38, were differently regulated by $GONH_2$ compared to GO, supporting possible diverse B cell activation paths. Moreover, co-culture experiments also suggest the functional ability of both GOs to activate B cells and therefore enhance the toxicity towards HeLa cancer cell line. Complete transcriptomic analysis on a B cell line highlighted the distinctive GO and $GONH_2$ elicited responses, inducing pathways such as B cell receptor and CD40 signaling pathways, key players for GrB secretion. B cells were regularly left behind the scene in graphene biological studies; our results may open new horizons in the development of GO-based immune-modulatory strategies having B cell as main actors.

1. Introduction

Graphene, a single layer of hexagonally-arranged carbon atoms, and graphene-based materials (GBMs), including graphene oxide (GO), the highly-oxidized form of graphene, are carbon nanomaterials with extraordinary physicochemical properties. GBMs are investigated for several breakthrough applications, including in biomedicine.[1-4] A critical parameter to evaluate when screening materials, including GBMs, for biomedical applications is the potential impact on the immune system.[5-9]

In this context, B cells are central to the immune response as they can secrete high-affinity antibodies against pathogens and can also act as antigen-presenting cells. [10] Maturation of B cells into plasma cells is modulated by different cytokines and co-stimulatory signals. In the presence of IL-21 stimulation, B cells can follow at least two distinct pathways during their activation: i) they undergo apoptosis in the absence of both B-cell receptor (BCR) engagement and T cell help;[11] and ii) they can differentiate into long-lived memory and antibody-secreting plasma cell in the presence of CD40 ligation by T cell, and either a BCR signal or a Toll-like receptor (TLR) signal. Recently, it was demonstrated that human plasma cells can express, and secrete the active form of the serine protease granzyme B (GrB),[12] therefore potentially acquiring cytotoxic proprieties.[13, 14] Moreover, several studies demonstrated that the interactions between GBMs and the immune cells depend on many factors correlated to their physicochemical properties including the functionalization.[10, 15, 16,17, 18] A study on isolated mice B cells reported increased cellular toxicity in cells treated with graphene alone.[19] Recently, we have shown the uptake of another type of graphene, few-layer graphene, by isolated mouse B cells.[20] We previously proposed the use of single-cell mass cytometry to dissect the immunological effects of GBMs on individual cells.[21, 22] Recently, we characterized and described a new functionalization of GO with ZnS-doped $AgInS_2$ quantum dots (GO-In) that enables the detection of the material in the indium channel (^{115}In),[23] allowing its high-throughput tracking by single-cell mass cytometry.[21] This new approach revealed the ability of GO-In to interact with human classical monocytes and, unexpectedly, B cells, showing high single-B-cell functional heterogeneity.[21] The interaction of GBMs with monocytes and monocyte-derived macrophages has been studied by us and others.[24-28] On the other hand, despite B cells play a fundamental role in the adaptive immune system for both humoral and cellular immunity,[29] their interactions with GBMs in terms of viability, functionality, anticancer activity, and transcriptomic profiling remains an unexplored, fertile land. In particular, these aspects and the interaction of graphene oxide and amino-functionalized graphene in the presence of the other 15 human primary immune cell types have never been explored. We cannot avoid the nature of immune cells, a complex pool of a wide variety of actors, each single cell type should be considered together and at the same time with all the other

immune cells. Moreover, none of these studies has been performed on human primary B cells and at a single-cell level analyzing three different cell subsets simultaneously applying a wide variety of assay: viability single-cell mass cytometry deep immune profiling, functional assays on a wide variety of cytokine and activation markers, cancer-cell killing activity assay and, moreover providing the full view on b cell transcriptomic profiling. Guided by our results on B cells graphene-oxide uptake[21], we aimed at filling a critical knowledge gap in the graphene biomedical scenario. We here show the results of all the assays mentioned above providing a comprehensive view of GBMs on B cells.

2. Results and Discussion

2.1 GO functionalization and characterization

In this study we used commercially available GO and GO-NH_2 (**Figure S1 & S2**). GO was prepared by the Hummers' method. The sheets have an average lateral size around 375 nm (**Figure S1c**). This GO was functionalized to introduce amino functions through derivatization with triethylene glycol diamine by epoxide ring opening (**Figure S2a**).[30] Transmission electron microscopy (TEM) (**Figure S1b and S2b**) and atomic force microscopy (AFM) (**Figure S1f & g and S2e & f**) images show that the functionalization process induced some aggregation of the sheets. The introduction of nitrogen was confirmed by X-ray photoelectron spectroscopy (XPS) as the characteristic peak of amines appeared at ~400 eV in the survey (**Figure S1d and S2c**). The oxidation state was also analyzed by XPS recording C1s spectra of the two materials (**Figure S1e and S2d**). The amine loading was 165 µmol/g according to the Kaiser test. Thermogravimetric analysis performed under inert atmosphere indicate that the thermal profile is different after the introduction of the amino groups, which is a sign that GO has been successfully functionalized (**Figure S2g**). Finally, the values of the zeta potential resulted in the same range between -40 to -50 mV (**Figure S2h**). However, little aggregation observed by TEM and AFM might influence such type of measurement.

2.2 GO and $GONH_2$ induce a specific GrB-mediated B cell response

We performed in-depth immune profiling at the protein and gene level, dissecting in detail the impact of GO and $GONH_2$ on B cells.

First, whole human peripheral blood mononuclear cells (PBMCs) were exposed to 25 and 50 µg/mL of GO or $GONH_2$ for 24 h. Concentration and time point were based on our previously reported data.[22] Both GO and $GONH_2$ resulted stable upon suspension in cell culture media (**Figure S3**). Viability evaluation on human PBMCs significantly showed a moderate increase of toxicity in cells treated with 50 µg/mL of GO, and no toxicity in $GONH_2$-treated cells (**Figure S4**). This difference is due to the specific graphene surface of each material and may be also due to the possible diverse

protein corona formation for the two materials which is critical for their behavior in biological systems as reported by previous groups for other materials.[4, 17, 31, 32]

No significant genotoxicity was observed for both materials at any concentration tested, as evident by real-time PCR analysis, DNA fragmentation assay, and H2AX DNA damage marker staining (**Figure S5 a-c**).

A broad immune profiling at the single-cell level was performed focusing specifically on B cells among the other 13 well-detected immune populations. An extended cytokine panel including IL-4, IL-6, and GrB (key B cell functional mediators) was applied by single-cell mass cytometry.[33, 34] A visualization tool for high-dimensional single-cell data based on the t-Distributed Stochastic Neighbor Embedding (t-SNE) algorithm (viSNE) was used to reduce the dimensionality of the data set.[35] $CD45^+$ events were analyzed by viSNE to cluster all the single-cell events into 13 populations according to 8 protein expression readouts used in the analysis (CD3, CD4, CD8, CD14, CD16, CD20, CD19, and CD123).[22] The viSNE analysis accurately identified helper and cytotoxic T cells (Th cells and CT cells, respectively), classical (C) and non-classical (NC) monocytes, myeloid dendritic cells (mDCs), plasmocytoid dendritic cells (pDCs), natural killer cells (NKs), and B cells (**Figure 1a**).

To deconvolute the different immune population composition after treatment with the materials we applied the sunburst software feature present on Cytobank (https://www.beckman.com/flow-cytometry/software/cytobank-premium/data-visualization).

We found that both GO and $GONH_2$ induced a reduction of the total monocyte content (**Figure S6a**). We confirmed our previous findings[22] on the ability of amino functionalized GO to induce monocyte activation mostly toward a M1 polarization response, as demonstrated by the increased and coherent production of classical M1 cytokines such as TNFα, IL6, and MIP1β (**Figure S6b**).[22] Moreover, the increased IL4 production may reflect transcriptional regulation of genes involved in TLR signaling pathways.[36] GO instead caused a broad, non-specific activation of monocytes triggering the production of most of the cytokines analyzed (**Figure S6c**).

To fill the knowledge gap on graphene B cell interactions and to study its possible impact, we applied a further viSNE analysis on the gated B cells ($CD3^-$ $CD19^+$ $CD20^+$) using as readouts CD27, CD38, and HLA-DR. The viSNE discrimination of B cells successfully identified the three major populations: i) naïve, ii) memory, and iii) plasma B cells (**Figure 1b**). Cisplatin was used as a marker of cell viability for all B cell subpopulations analyzed, revealing significant differences in terms of cytotoxicity exerted by the two materials as shown in the histogram reporting the LD median intensity on B cell immune subsets identified with CyTOF (**Figure 1c, d, e**). GO and $GONH_2$ stimulated similarly the expression of TNFα in naïve, memory, and plasma B cells, which act at different steps

in B cell differentiation (**Figure 1f, g**). IL-6 production was induced by GO in naïve, and by both GO and $GONH_2$ in memory B cells (**Figure 1f**). While IL-2 production was significantly affected by both GO and $GONH_2$ in naïve and memory B cells, IL-4 production was induced exclusively by $GONH_2$ in memory and plasma B cells as highlighted in the heat map (**Figure 1g, h**). Functionalized $GONH_2$ significantly (p<0.05) enhanced GrB production in both plasma and memory B cells with a stronger induction compared to GO (**Figure 1g, h**). To confirm these data, we performed GrB gene expression analysis (*GZMB*) and protein secretion of human primary B cells treated or untreated with GO and $GONH_2$. Intriguingly, both GO and $GONH_2$ significantly induced the expression and secretion of GrB (**Figure S7a, b**). Granzymes are closely related serine proteases that represent key components of the cytotoxic granules of natural killers (NKs) and cytotoxic T lymphocytes (CTLs).[14] GrB is a 32 kDa protein released via granule exocytosis and it initiates perforin-dependent death in target cells by cleaving caspase-3 at aspartic acid residues, as well as by activating additional cytotoxic pathways.[37, 38] GrB secreting B cells are believed to exert an innate-like function including a targeted killing function.[39] Moreover, GrB may play a role during antigen cross-presentation function of B cells.[13]

To further explore the function played by GO and $GONH_2$ on B cells, after material exposure, we analyzed cell viability and the expression of specific markers like CD38, CD138, CD80, and CD69 on isolated B cells employing flow cytometry. $GONH_2$ showed a higher biocompatibility on B cells compared to GO, which induced a significant increase of necrotic cells (20%) (**Figure 2a, b**). No significant differences were detected for apoptotic cells after treatment with the materials (**Figure 2c**). Flow cytometry data showed that 4 to 8% of B cells treated with GO or $GONH_2$ loose CD20 expression, expressing only CD19 (**Figure 2d**). The loss of CD20 is commonly associated with the activation of B cells in plasmablasts and plasma cells.[40] Both GO and $GONH_2$ were able to activate the expression of CD69 that is known as an early activation marker for leukocytes, and transiently expressed by activated B cells[41] (**Figure 2e**), and CD80, a well-known marker linked with CD86 expression and the early B cell activation[42] (**Figure 2f**). Intriguingly, CD69 was strongly enhanced by GO, while $GONH_2$ enhanced CD80 expression (**Figure 2e, f and S8**). These data suggest possible difference in GO and $GONH_2$-mediated B cell activation.

Thus, only $GONH_2$ increased the expression of CD38 and CD138 (**Figure 2g, h**). Both CD38 and CD138 drives B cell survival and differentiation into plasma cells.[43] Overall, the single-cell data and the flow cytometry data suggest that GO and $GONH_2$ significantly drives B cell activation and differentiation.

Furthermore, as a proof of concept, to evaluate whether GrB released by GO/$GONH_2$-treated B cells may exert an antitumor effect, primary B cells were co-cultured with HeLa cell line (cervical cancer

cells) and treated with GO or $GONH_2$, or left untreated. All materials induced a significant increase of cell death, compared to controls, as measured by lactate dehydrogenase (LDH) assay, while no changes were detected in HeLa cells or B cells treated with GO or $GONH_2$ (**Figure 2i**). These data are a proof of principle to support the concept that GrB production by GO/$GONH_2$-exposed B cells may result in enhanced cancer cell killing.

2.3 Whole-genome transcriptomic analysis of Raji B cell line.

To increase our understanding on the mechanism on the discovered interaction of GO and $GONH_2$ with B cells, we performed genome-wide transcriptomic analysis on the B cell line model Raji. A total of 14595 unique genes were analyzed. This unbiased approach allowed us to identify functional biological processes modulated by GO and $GONH_2$ in Raji B cells.

B cells Raji cell line, were incubated with GO or $GONH_2$ (50 μg/mL, 24 h) at the same conditions used for the previous experiments. To compute the probability of genes being differentially expressed, we fit a linear regression model of each gene using limma (see Methods). Differentially expressed genes (DEG) were defined using a cutoff of 0.005 for nominal *p* value and a false discovery rate (FDR) of 0.1 (see **Table S1**). The Volcano plots display the magnitude of the perturbations induced by the materials (**Figure 3a**). Representative genes modulated by each material are labeled in both plots. Overall, following the treatment with $GONH_2$ and GO, 496 and 619 transcripts were altered in $GONH_2$ and GO-treated samples, respectively. Among them, 197 transcripts were exclusively up-regulated by $GONH_2$ and 183 by GO. In contrast, 148 and 285 transcripts were uniquely down-regulated in $GONH_2$ and GO, respectively (**Figure 3b**). Seventy and 81 transcripts were respectively up-regulated and down-regulated by both materials (Figure 3b).

To provide a functional interpretation of the transcriptional changes, we performed functional analyses using canonical pathways from Ingenuity Pathway Analysis (IPA) (see T**able S2 and Figure S9 and S10**). The top 20 most differentially affected canonical pathways (according to statistical significance) for each material are represented in **Figure 3c**, and ordered according to the enrichment *p* value in $GONH_2$. If a pathway was significantly enriched in the comparison related to one material (e.g., $GONH_2$ vs CTRL), it was also displayed for the other one (GO vs CTRL). Representative genes labeled in the Volcano plots are displayed in heatmap in each replicate (**Figure 3d**) and labeled according to functions (in this case B-cell related and DC-related functionally similar canonical pathways were aggregated, see also **Table S2**).

This analysis revealed that, although the number of overlapping genes among the two materials was limited using the pre-defined significance cut-off, the ultimate effect on several biological pathways was similar, although not identical. Strikingly, among the top modulated pathways, there were three

canonical pathways related to B cell activation, (i.e., B cell receptor signaling, Systemic Lupus Erythematosus (SLE) in B cell signaling and PI3K signaling in B cell lymphocytes) with an enrichment of upregulated transcripts. A representation of B cell receptor signaling pathway modulation is provided in Figure 4.

The interferon (IFN) signaling pathways (JAK-STAT signaling, and role of JAK1, JAK2, and TYK2 in IFN signaling,) were also coherently upregulated by both materials (**Figure 3c and Figure 5a**). Cancer-related pathways were dysregulated by both GO and $GONH_2$ (**Figure 3b**) due to the modulation of genes involved in cellular growth, such as EGR2, KRAS, MAP2K1, and PIK3C2A, up-regulated by $GONH_2$, and PIK3CG and MAP2K2, upregulated by GO reflecting the pro-activation effect exerted by these materials. In fact, the ERK-MAPK signaling pathway, which controls several cellular functions including proliferation in normal cells, immune cells, and cancer cells [44], was significantly upregulated by both materials. The ERK-MAPK signaling pathway activation was further confirmed by western blot of primary B cells after GO or $GONH_2$ treatment, showing significantly increased phosphorylation of p44 MAPK (ERK1/2) (**Figure S11**).

Conversely, and perhaps reassuring, the classic proto-oncogene MYC was inhibited by both materials. Despite these analogies some differences emerge between the effect induced by GO and its functionalized form. The TNFR2 signaling pathway (involved in the TNFα signaling) was significantly activated only by GO (**Figure 3c**), in line with the highest production of TNFα by GO as compared with $GONH_2$, detected by the CyTOF analysis. (**Figure 1f-h**).

The CD40 signaling pathway, moreover, was activated only by GO, and, to a lesser extent by $GONH_2$ (**Figure 3c-d and Figure 5b**). In particular, only GO induced upregulation of CD40. Remarkably, CD40 activation by CD40L (expressed by activated T cell), is required to induce long-lived memory and antibody-secreting plasma cells, while absence of CD40 ligation induces B cells to secrete GrB.[39] Therefore, transcriptomic data might explain the divergent effect on primary B cell differentiation observed by CyTOF and flow cytometry analysis (**Figure 1d-e and Figure 2c**). As GBMs also induces activation of T cells,[22] is it possible that in the cellular cultures (PBMCs) used in CyTOF and flow cytometry, CD40L expressed by activated T cell might have induced B cell differentiation toward plasma cells (CD20-), observed for both GO and $GONH_2$. However, the upregulation of CD40 by GO might have induced the expression of GrB as CD40 activation by CD40 ligand inhibits GrB expression in B cells.[39] This remains a speculation as it is currently poorly understood how GrB expression is modulated in plasma cells. Other cytokines such as IL15 might be involved in the translation of GrB proteins in B cells.[12] Remarkably, functional data in experimental models are lacking as mice plasma cells do not express GrB.[12]

Furthermore, differentiation into plasma cells is also induced by TLR activation,[45, 46] a pathway modulated by GO stimulation (see **Table S2, Figure S9 and S10**).

We also evidenced an increased expression of CD19 in the $GONH_2$-treated Raji B cells, in line with the flow cytometry data which detected a proportional enrichment of CD19+ CD20- cells following $GONH_2$ incubation (**Figure 2d**). In addition, both materials induced upregulation of chemoattractant cytokines such as CCL chemokines CCL3, CCL4L1/L2, and CCL22, which are important for innate and adaptive cells cross talk. A chemokine network constructed using genes differentially modulated by either GO or $GONH_2$ is represented in **Figure 6**; genes significantly modulated by either GO (**Figure 6a**) or $GONH_2$ (**Figure 6b**) are highlighted.

The robustness of our functional analysis was confirmed by RMDB**,** a method implemented here to comprehensively summarize and display differentially enriched pathways using 32 open-source databases (ConsunusPathDB) (see Methods for details).[47] Such analysis confirmed and expanded the results retrieved using IPA (**Figure 5 and 6**): B cell receptor activation and IFN signaling activation was detected in both GO and $GONH_2$ comparisons, while CD40/CD40L, TLR and TNRF2 activation only in GO. However, this approach also detected activation of IL-2 signaling by GO and $GONH_2$.

3. Conclusions

The extensive investigation by high dimensional immune profiling on single-cell mass cytometry, a wide variety of functional assays and transcriptomic analysis presented here, showed that B cells interact with both GO and $GONH_2$ and are influenced in their functionality. We implemented the viSNE analysis of single-cell mass cytometry focusing on i) naïve, ii) memory, and iii) plasma B cells, with an extended cytokine panel including IL-4, IL-6, and GrB, critical B cell functional mediators. $GONH_2$, in particular, showed a specific induced production of several cytokines such as TNF, IL-4, IL-6, and IL-2 and, interestingly, granzyme B. These data were confirmed by activation markers screening by flow cytometry, real time qPCR and Cytometric bead array (CBA) on granzyme B and, further elucidated by the transcriptome analysis, therefore suggesting a $GONH_2$-mediated activation of BCR and CD19 signaling. BCR signaling activation was also confirmed by the ERK1/2 increased phosphorylation induced by both GO and $GONH_2$. The single-cell screening together with the transcriptomic analysis revealed a new potential application of these materials, may be being able to stimulate a cytotoxic like function mediated by induction of GrB production by B cells. Our findings clearly indicated the GO and $GONH_2$ in particular immunomodulatory properties, and their action towards GrB-secreting B cells. With the activation of other lymphocytes such as monocytes, this should be critically considered in developing new graphene-based biomedical tools, in particular when envisaging a contact with blood immune cells. The ability of GO, even enhanced by $GONH_2$,

to stimulate B cell activation with an induction of GrB production, might be of high interest for further medical applications and studies, in particular in the context of cancer research as B cells specific cancer cell killing enhancer, or as immunomodulatory approach based on adoptively transfer of GrB^+ B cells, as recently proposed.[14] Our findings, while confirming that both GO and $GONH_2$ bear strong pro-activating properties, further unveiled the ability of $GONH_2$ to induce a B cell receptor signaling activation unpaired with CD40 over-expression/signaling activation. Such signaling dysregulation might represent a permissive condition for the production of GrB following $GONH_2$ treatment. GrB^+ B cells with cytotoxic properties may trigger an early induction of antigen-specific, cytotoxic immune responses which might be beneficial for immune-mediated cancer rejection.[14].

Indeed, GrB secreting B cells might play a significant role in the early phase of antiviral immune responses, in the regulation of autoimmunity, and in cancer cell killing in the initial phase of neoplastic transformation (cancer immunosurveillance),[13] and GrB production is acquired quickly and much earlier than the property of producing antibodies. In fact, the implementation of adoptive therapy based on GrB-expressing B cells or their *in vivo* induction using IL-21 have been proposed as potential cancer immunotherapeutic approaches. [13, 14]

In conclusion, by considering our recently introduced nanoimmunity-by-design concept,[9] our findings on B cells, one of the key player of the adaptive response, open up two new windows on the graphene scenario: i) new strategies for graphene-mediated immunotherapy, and ii) a new high-dimensional multi-cellular and multi-parametric approach for the safe assessment of GBMs based on the specificity of the B cell-immune reactions.

In this context, out study lay new foundations for graphene-based biomedical and immune-application, with B cells as main actors.

4. Experimental Section

Material preparation

GO and $GONH_2$ were obtained from NanoInnova (Spain). Aqueous suspensions were prepared by dispersing the powder in water and sonicating for 20 min prior to use. TGA was performed on a TGA1 (Mettler Toledo) apparatus from 30 °C to 900 °C with a ramp of 10 °C·min^{-1} under N_2 using a flow rate of 50 mL·min^{-1} and platinum pans. Transmission electron microscopy (TEM) analysis was performed on a Hitachi H600 with an accelerating voltage of 75 kV. The samples were dispersed in water/ethanol (1:1) at a concentration of 16 μg/mL and the suspensions were sonicated for 10 min. Ten microliters of the suspensions were drop-casted onto a carbon-coated copper grid (Formvar film 300 Mesh, Cu from Electron Microscopy Sciences) and left for evaporation under ambient conditions.

AFM height images were acquired using a Multimode 8 system (Bruker, UK) in tapping mode, operating at room temperature. OTESPA silicon cantilevers (Bruker, UK) with a resonance frequency of 300 kHz and a nominal force constant of 42 Nm^{-1} were used. AFM samples were prepared by drop casting onto a freshly cleaved mica [previously coated with 20 μL of 0.01 % of poly-L-lysine (Sigma-Aldrich, UK) for the non-functionalized GO sample], using 20 μL of the corresponding GO and $GONH_2$ dispersions (100 μg/mL). Unbound materials were removed by washing with 2 mL of MilliQ water, and then dried overnight at 37 °C. The acquired AFM height images were processed using the Nanoscope Analysis software (version 1.4, Bruker, UK) to elucidate the thickness distribution of the GO samples. X-ray photoelectron spectroscopy (XPS) was performed on a Thermo Scientific KAlpha X-ray photoelectron spectrometer with a basic chamber pressure of 10^{-8}-10^{-9} bar and an Al anode as the X-ray source (1486 eV). The samples were analyzed as powder pressed onto a scotch tape (3MTM EMI Copper Foil Shielding Tape 118). Spot size of 400 μm was used for analysis. The survey spectra are an average of 10 scans with a pass energy of 200.00 eV and a step size of 1 eV. For each sample, the analysis was repeated three times. A flood gun was turned on during analysis. Zeta potetial measurements were performed three times at 25 °C with 120 s equilibration time using a Malvern Zetasizer Nano ZS (Malvern Instruments). Stock solutions (at 1 mg/mL) of the two materials were diluted in milli-Q® water to about 0.1 mg/mL. All materials were endotoxin free, as previously reported.[48]

Stability of GO and $GONH_2$ in cell culture media

An aliquot of GO or $GONH_2$ solution at a concentration of 1 mg/mL in Milli-Q® water was first prepared by 10 min bath sonication. Subsequently, the dispersion was diluted in cell media under sterile conditions and sonicated for 10 min, obtaining a final concentration of 50 μg/mL. Photos were taken after bath sonication and incubated after 2 hours and overnight.

Isolation of PBMCs

Buffy coats from informed healthy donors (aged 25–50 years) were obtained from the University Hospital Tor Vergata and University Hospital of Sassari. Informed signed consent was obtained from all the donors. PBMCs were isolated from buffy coat by Ficoll-Paque PLUS (GE Healthcare) density gradient centrifugation. B cells were isolated from PBMCs using EasySep™ Human B Cell Isolation (Stem Cell). PBMCs and isolated B cells were daily maintained in RPMI-1640 medium added with

FBS 10% and 1% of penicillin/streptomycin solution. At least 1×10^6 cells for sample in each experiment were used. All the experiments were performed in biological and technical triplicate.

Cell culture

Raji (B cell line) were supplied by the ATCC (American Type Culture Collection) and tested for mycoplasma contamination. Cells were daily maintained in RPMI-1640 medium added with FBS 10% and 1% of penicillin/streptomycin solution. At least 1×10^6 cells for sample in each experiment were used. All the experiments were performed in biological and technical triplicate. B cells were used for gene expression experiments. B cells were incubated with GO or $GONH_2$ (50 μg/mL) for 24 h, or left untreated.

Analysis of the B cell behavior after graphene treatment using CyTOF2

Single-cell mass cytometry analysis was performed using purified PBMCs obtained as described above. PBMCs were seeded in a six multi-well plates (3×10^6 cells/well) and treated with GO, and $GONH_2$ at the fixed concentration of 50 μg/mL for 24 h or left untreated. For the detection of cytokines, brefeldin A was added 5hrs before the incubation end. After the incubation time, cells were harvested and washed with phosphate-buffered saline (PBS). Before the staining, cells were incubated for 5 min with cisplatin-194Pt to a final concentration of 1 μM. Cells were then stained using Maxpar Human Peripheral Blood Phenotyping and Human Intracellular Cytokine I Panel Kits (Fluidigm, CA, USA) following the manufacturer staining protocol for cell surface and cytoplasmic/secreted markers. Briefly, cells were harvested and resuspended in 50 μl of Maxpar Cell Staining Buffer into 15 mL polystyrene tubes for each sample. The surface marker antibody cocktail (dilution of 1:100 for each antibody) was added to each tube (final volume 100 μl). Samples were mixed and incubated for 30 min at room temperature. After incubation, the samples were washed twice with Maxpar Cell Staining Buffer. Cells were then fixed by adding 1 mL of Maxpar Fix and Perm Buffer to each tube and incubated for 10 min. After incubation, cells were washed twice with Maxpar Fix and Perm Buffer and centrifuged for 5 min at 800×g. Cells were then suspended in 50 μL of Maxpar Fix and Perm Buffer and incubated as described above with cytoplasmic/secreted antibody cocktail (dilution of 1:100 for each antibody final volume 100 μL). Afterwards, cells were washed twice with Maxpar Cell Staining Buffer and incubated with Cell-ID Intercalator-Ir solution at the final concentration of

125 nM into Maxpar Fix and Perm Buffer for 5 min. Each sample was then washed twice with Maxpar Cell Staining Buffer and suspended with 2 ml of ultrapure water. Before the data acquisition, each sample was filtered into 5 mL-round bottom polystyrene tubes with a 30 μm cell strainer cap to remove possible cell clusters or aggregates. Data were analyzed using mass cytometry platform CyTOF2 (Fluidigm Corporation, CA, USA).

Gating strategy applied

The CyTOF data analysis was performed according to the methods described by Orecchioni *et al.* [22] and Bendall *et al*.[49] Summarizing, normalized, background subtracted FCS files were uploaded into Cytobank for the analysis. Specific PBMC subsets and subpopulations were identified using the following strategy: T cells (CD45+ CD19- CD3+), T helper (CD45+ CD3+ CD4+), T cytotoxic (CD45+ CD3+ CD8+), T naive (CD45RA+ CD27+ CD38− HLADR−), T effector (CD45RA+ CD27− CD38− HLADR−), and activated (CD38+ HLADR+), B cells (CD45+ CD3- CD19+), B naive (HLADR+ CD27−), B memory (HLADR+ CD27+), plasma B (HLADR− CD38+), NK cells (CD45+ CD3− CD19− CD20− CD14− HLADR− CD38+ CD16+), Classical monocytes (CD45+ CD3− CD19− CD20− HLADR+ CD14+), Non classical monocytes (CD45+ CD3− CD19− CD20− HLADR- CD14- CD16+), mDC (CD45+ CD3− CD19− CD20− CD14− HLADR+ CD11c+ CD123−), and pDC (CD45+ CD3− CD19− CD20− CD14− HLADR+ CD11c− CD123+). Cytobank allowed the realization of the heat map visualization comparing marker fluorescence of the treated populations with mean fluorescent intensity vs. the untreated control. viSNE tool was exploited. viSNE, a cytometry analysis tool implemented in Cytobank, uses t-stochastic neighbor embedding (t-SNE) portraying single cells in a two- or three-dimensional plot, on the basis of their relationships. Nine cell surface markers were used to draw the viSNE map for the Maxar PBMCs staining: CD3, CD4, CD8a, CD11c, CD14, CD16, CD19, CD20, CD123, and HLADR. The specific viSNE on B cells populations were performed on the gated CD3- CD19/CD20+ events; to construct the viSNE map CD27, CD38, and HLADR were applied. The cytokine data analysis was performed exploiting viSNE tool. Heat maps and plots report the median signal intensity (MSI) of the analyzed cytokines (IL-2, IL-4, IL-5, IL-6, MIP1β, TNF and GrB).

Viability and activation assays and cytokines expression on ex vivo PBMCs

The apoptosis assay was performed using Annexin V/ PI labeling. Briefly, PBMCs were incubated with 50 µg/mL of GO and $GONH_2$ for 24 h. As positive control, cells were incubated for few seconds with 70% of ethanol, while samples incubated with cell medium alone was used as negative control. The cells were stained with Annexin V/PI staining, incubated for 20 min in the dark and suspended in Annexin V 1X buffer. PBMCs were then incubated for 24 h with GO and $GONH_2$ (50 µg/mL) and percentage of necrotic cells was assessed using 7AAD (eBioscience) labeling. The cytotoxicity was evaluated by flow cytometry (FACS CANTO II, BD Biosciences, Mountain View, CA, USA).

B cell activation assays

B cells were isolated as previously described and incubated with GO or $GONH_2$ (50 µg/mL) for 24 h, or left untreated. Lipopolysaccharides (LPS 2 µg/mL), Concanavalin A, (ConA, 10 µg/mL) was used as positive controls for B cells activation. Cells were stained to identify activation markers expression (CD69, CD38, CD138, and CD80; eBioscience). Staining with fluorochrome-conjugated monoclonal antibodies was performed in the dark for 20 min at 4 °C. After washing, cells were analyzed by flow cytometry using LSR II (BD Bioscience).

B cell killing assay

HeLa cell line was obtained by ATCC and cultured following standard conditions with DMEM (Gibco) supplemented with 10% FBS and 1% penicillin/streptomycin solution. HeLa cells (1×10^5 cells/well) were seeded in 24-well plate. After 2 h, B cells (2.5×10^5 cells/well) were added. HeLa cells cultured alone or co-cultured with B cells were then incubated with GO or $GONH_2$ (50 µg/mL) for 24 h, or left untreated, and cell viability was assessed by LDH assay. B cells alone were also used as controls. LDH release was measured using the CyQUANT™ LDH Cytotoxicity Assay (Thermo Fischer) following the manufacturer's protocol. Absorbance was measured at 490 nm and 680 nm using a Spectramax 2213 spectrophotometer (Molecular Devices).

Immunoblotting

B cells were isolated as previously described and incubated with GO or $GONH_2$ (50 µg/mL) for 24 h, or left untreated. Cells were lysed in RIPA buffer [20 mM Tris-HCl (pH 7.5), 150 mM NaCl, 1

mM Na2EDTA, 1 mM EGTA, 1% NP-40, 1% sodium deoxycholate, 2.5 mM sodium pyrophosphate, 1 mM beta-glycerophosphate, 1 mM Na3VO4, 1 µg/ml leupeptin] containing 1mM phenylmethanesulfonyl fluoride, 1× protease inhibitor cocktail (Roche), and PhosSTOP (Sigma-Aldrich). Immunoblotting was performed using a rabbit monoclonal anti-human p44/42 MAPK (p-Erk1/2), (Thr202/Tyr204) #9101 and anti-human p44/42 MAPK (Total-Erk1/2) (137F5) #4695 from Cell Signaling Technology and a rabbit anti–glyceraldehyde-3-phosphate dehydrogenase (GAPDH) antibody from Cell Signaling Technology. Intensity of bands was calculated using the ImageJ (NIH, version 1.8.0_201) software and normalized based on GAPDH and total ERK1/2.

Quantitative Real Time PCR

Human isolated B cells (0.5×10^6 cells per well) treated as as previously described and incubated with GO or $GONH_2$ (50 µg/mL) for 24 h, or left untreated were transferred into 500 µl Qiazol. Supernatants were harvested and used for further analysis. RNA was extracted by a Qiazol/RNAeasy micro kit hybrid protocol (cat# 74004, Qiagen). cDNA was made using Omniscript reverse transcriptase (cat# 205111, Qiagen). Real time PCR reactions were performed according to the RT2 SYBR green gene expression assay protocol (cat# 330501 Qiagen). RT2 SYBR Green qPCR master mix and premade RT² qPCR Primer Assays (Qiagen) for human *GZMB* (cat# PPH66781A-200) and GAPDH (cat# PPH00150F-200).

Cytokine bead array

Supernatants harvested as above described were analyzed by BD CBA Flex Sets (BD Biosciences) for human GrB (cat# 560304).

Genotoxicity assessment by RT qPCR

Cells (5×10^6 cells) were harvested and RNA was extracted from cells by using the Machery Nagel RNA isolation kit. iScript cDNA synthesis kit (Bio-Rad.UK) was used according to the kit's protocol for cDNA synthesis from 1 µl of RNA sample. Real-timePCR was performed using the CFX-96 Real TimeSystem (Bio-Rad.UK) with SSO Advanced SYBER Green (Bio-Rad.UK) in 20 µl reactions using the following conditions: 95 °C for 3 min, 1 cycle: 95 °C for 10 sec, 60 °C for 30 sec,-repeated for 40 cycles. *GAPDH* was used as reference gene and gene expression levels were normalized to untreated control groups.

DNA fragmentation assay

For DNA fragmentation assay, PBMCs were seeded into 6 well plates (0.5-1×10^6 cells per well). After seeding, the cells were treated with GO or $GONH_2$ and incubated at 37 °C and 5% for 24 h. As positive control, cells were treated with 30% DMSO. After 24 h, cells were collected in 1.5 ml microcentrifuge tubes and centrifuged at 200×g for 10 min. Cell pellets were washed with PBS and centrifuged again at 200×g for 5 min. After washing, the pellets were used in the DNA Ladder Detection Kit (Abcam), according to the kit protocol. At the end, samples were run in 1.8% agarose gel for 75 V for 2 h. After running, the gel was stained according to the kit protocol and visualized with the Gel Doc EZ System (BIO-RAD) and gel images were analyzed in ImageJ software.

DNA damage assessment

In order to determine DNA damage and repair levels, cells (1×10^6 cells) were collected and washed two times by Dulbeccos Phosphate Bufered Saline (DPBS) (Life Technologies) Later, cells were permeabilized with Tween20 containing PBS which was followed by 1 h incubation with anti-phospho H2AX antibody in 1% bovine serum albumin containing PBS. Prepared samples were analyzed with BD Accuri Plus flow cytometer. Data were analyzed with BD Accuri Plus software.

Gene expression impact of GOs on B cells

Total RNA was extracted and purified from B cells (Raji (B cell line) using the RNAeasy mini kit (Qiagen, Valencia, CA, USA). RNA purity was assessed by spectrophotometric analysis and integrity by microfluidic molecular sizing using the Bioanalyzer 2100 (Agilent). An RNA Integrity Number (RIN) >/= than eight was required. RNA (1 μg) was converted in cRNA and labeled (Illumina totalPrep RNA amplification kit, Ambion). Biotinylated cRNA was hybridized onto the Illumina HumanHT-12 v4 (Illumina, Inc., San Diego, CA, USA). The Illumina HumanHT-12 v4 interrogates the expression of 47323 probes derived from the National Center for Biotechnology Information Reference Sequence RefSeq Release 38 and other sources. Probe intensity and gene expression data were generated using the Illumina GenomeStudio software V2011.1 (Gene Expression Module V1.9.0). Pre-normalization expression data was read into R using the lumiR function from the "lumi" package (v2.34).[50] Probe to gene annotation was added using the lumiHumanAll.db package (v1.22), and non-matching probes were discarded.

Expression was quantile normalized and log2 transformed using lumiN and lumiT functions, respectively. Flat probes were dropped, and the data was saved and a Rdata object containing the lumi expression sets (pre and post normalization) and the probe expression matrix along with sample

annotation. Probes targeting the same gene were averaged and a final matrix of 14, 595 unique genes was obtained. The matrix used for the analysis is available as Electronic Supplementary Information**.** Differential gene expression analysis was performed using limma (linear model for microarray data) (v3.38).[51]

Volcano plots of differential expressed genes were plotted using the EnhancedVolcano package (v1.0.1) Differentially expressed genes (DEGs) were defined using a nominal p value < 0.005 and a false discovery rate (FDR) p value < 0.1 using the Benjamini-Hochberg method.[52] These lists of genes were used for pathway analysis.

Enriched pathways were plotted using ggplot2. (v3.2.1). For pathway analysis, we used to orthogonal methods. First, we used Ingenuity Pathway Analysis (IPA) (www.qiagen.com). IPA is closed-source software containing curated biological pathways called canonical pathways.

In addition to IPA, to increase robustness of the analysis, we implemented a systematic pathway analysis method (called here RMDB) based on open-source databases. First, we determined enriched pathways using ConsensusPathDB. [47, 53] ConsensusPathDB integrates interaction networks of humans including complex protein-protein, genetic, metabolic, signaling, gene regulatory and drug-target interactions from 32 public resources including KEGG,[54, 55] BioCarta,[55] PID, Reactome,[56] WikiPathways [57] etc. into a unique interaction network with complementary non-redundant type of edges.

The advantage of using ConsensusPathDB over a popular tool like DAVID [58] is that it provides the option to search through multiple databases (different types of interactions) to find enriched pathways unlike DAVID which uses only the KEGG database. Moreover, unlike IPA, Consensus PathDB is a free open source software available for such enrichment analysis. However, one of the issues with Consensus PathDB is that the same enriched pathway might appear from multiple different databases. Hence, our first goal was to locate such redundant pathways. We traversed through the list of all enriched pathways and for each such pathway (p_i), we identify other pathways whose name is either a substring or a super-string of p_i and the set of differentially expressed genes (DEG) of p_i is either a subset or a superset of the name-matched pathways (since both these pathways capture the same underlying biological function). Once we have identified all such pathways, which are similar to p_i, we kept only one non-redundant pathway i.e. the pathway which has the largest set of DEGs. Another issue is that there is a plethora of enriched pathways (after filtering redundant ones) obtained from Consensus PathDB, but these enriched pathways belong to certain classes such as Immune related pathways, Transcription/Translation related pathways, disease specific pathways etc. So, we next performed a clustering operation on this set of enriched pathways to group functionally equivalent pathways together. For this purpose, we look at the set of DEG associated with pathway p_i, say g_i =

$\{g^1, g^2, \ldots, g^n\}$, and estimate its similarity with any other pathway $p_j \in P$, by calculating the Jaccard coefficient between g_i and g_j. Mathematically this can be written as:

$$S(p_i,p_j) = |g_i \cap g_j| / |g_i \cup g_j|$$

Here the function |.| calculates the cardinality of the set, $S(p_i,p_j)$ represents the Jaccard coefficient and can take values between [0,1], where 0 means no similarity and 1 means that both the pathways have the same set of DE genes. We use the DEG associated with a pathway to estimate similarity based on the notion that similar set of genes should be associated with nearly similar functionality. After estimating S(.,.) for all pathway pairs, we obtain the adjacency matrix (S) of similarity. We next use a popular clustering technique called the Louvain method [59] to identify functionally similar groups of pathways. We then rank all the pathways in each cluster based on their statistical significance i.e. p values (from smallest to largest).

Supporting Information

Supporting Information is available from the Wiley Online Library or from the corresponding authors.

Acknowledgements

This work was partly supported by the European Union's Horizon 2020 research and innovation programme under the Marie Sklodowska-Curie grant agreement no. 734381 (CARBO-IMmap) and FLAGERA JTC Graphene 2015 (G-IMMUNOMICS project), and the Agence Nationale de la Recherche (ANR) through the LabEx project Chemistry of Complex Systems (ANR-10-LABX-0026_CSC). The authors wish to thank C. Royer and V. Demais for TEM analyses at the Plateforme Imagerie in Vitro at the INCI (Strasbourg, France), F. Rodrigues for AFM analysis and L. Newman for Raman measurements.

Author contributions

L.G.D. conceived the idea and coordinated the work. D.B. supervised the trascriptomics analysis. A.B. supervised the graphene production and characterization.

M.O., and L.F., implemented the experiments with help from V.B., C.F., D.R., S.G., R.S., M.Z. and C.G.

M.O, L.F and R.M. analyzed and interpreted the data with contributions from L.G.D., D.B., W.H., A.B. C.M.M., A.Y. and B.Z.

L.G.D., D.B., M.O. and L.F. wrote the manuscript with contributions from all authors.

Conflict of interest

The authors declare no conflict of interest.

References

1. G. Brumfiel, *Nature*, 2009, **458**, 390-391.
2. A. K. Geim and K. S. Novoselov, *Nat Mater*, 2007, **6**, 183-191.
3. A. K. Geim, *Science*, 2009, **324**, 1530-1534.
4. C. Weiss, M. Carriere, L. Fusco, I. Capua, J. A. Regla-Nava, M. Pasquali, J. A. Scott, F. Vitale, M. A. Unal, C. Mattevi, D. Bedognetti, A. Merkoci, E. Tasciotti, A. Yilmazer, Y. Gogotsi, F. Stellacci and L. G. Delogu, *ACS Nano*, 2020, **14**, 6383-6406.
5. S. P. Mukherjee, M. Bottini and B. Fadeel, *Front Immunol*, 2017, **8**, 673.
6. L. Fusco, A. Gazzi, G. Peng, Y. Shin, S. Vranic, D. Bedognetti, F. Vitale, A. Yilmazer, X. Feng, B. Fadeel, C. Casiraghi and L. G. Delogu, *Theranostics*, 2020, **10**, 5435-5488.
7. A. Gazzi, L. Fusco, A. Khan, D. Bedognetti, B. Zavan, F. Vitale, A. Yilmazer and L. G. Delogu, *Front Bioeng Biotechnol*, 2019, **7**, 295.
8. S. Keshavan, P. Calligari, L. Stella, L. Fusco, L. G. Delogu and B. Fadeel, *Cell Death Dis*, 2019, **10**, 569.
9. L. Fusco, A. Gazzi, M. Orecchioni, S. Ferrai G. Franzoni, J. S. Yan M. Rieckher, G. Peng M. A. Lucarelli, I. A. Vacchi, N. D. Q. Chau, A. Criado, A Istif, D. Mancino, A. Dominguez, H. Eckert, E. Vazquez, T. Da Ros, P. Nicolussi, V. Palermo, B. Schumacher, G. Cuniberti, Y. Mai, C. Clementi, M. Pasquali, X. Feng, K. Kostarelos, A. Yilmazer, D. Bedognetti, B. Fadeel, M. Prato, A. Bianco, L. G. Delogu, *JPhys Materials*, 2020.
10. K. L. Rock, B. Benacerraf and A. K. Abbas, *J Exp Med*, 1984, **160**, 1102-1113.
11. H. Jin, R. Carrio, A. Yu and T. R. Malek, *J Immunol*, 2004, **173**, 657-665.
12. W. Xu, P. Narayanan, N. Kang, S. Clayton, Y. Ohne, P. Shi, M. C. Herve, R. Balderas, C. Picard, J. L. Casanova, J. P. Gorvel, S. Oh, V. Pascual and J. Banchereau, *Eur J Immunol*, 2014, **44**, 275-284.
13. M. Hagn, E. Schwesinger, V. Ebel, K. Sontheimer, J. Maier, T. Beyer, T. Syrovets, Y. Laumonnier, D. Fabricius, T. Simmet and B. Jahrsdorfer, *J Immunol*, 2009, **183**, 1838-1845.
14. M. Hagn and B. Jahrsdorfer, *Oncoimmunology*, 2012, **1**, 1368-1375.
15. J. Russier, E. Treossi, A. Scarsi, F. Perrozzi, H. Dumortier, L. Ottaviano, M. Meneghetti, V. Palermo and A. Bianco, *Nanoscale*, 2013, **5**, 11234-11247.
16. M. Orecchioni, D. A. Jasim, M. Pescatori, R. Manetti, C. Fozza, F. Sgarrella, D. Bedognetti, A. Bianco, K. Kostarelos and L. G. Delogu, *Adv Healthc Mater*, 2016, **5**, 276-287.
17. B. Fadeel, C. Bussy, S. Merino, E. Vazquez, E. Flahaut, F. Mouchet, L. Evariste, L. Gauthier, A. J. Koivisto, U. Vogel, C. Martin, L. G. Delogu, T. Buerki-Thurnherr, P. Wick, D. Beloin-Saint-Pierre, R. Hischier, M. Pelin, F. Candotto Carniel, M. Tretiach, F. Cesca, F. Benfenati, D. Scaini, L. Ballerini, K. Kostarelos, M. Prato and A. Bianco, *ACS Nano*, 2018, **12**, 10582-10620.
18. M. Orecchioni, C. Menard-Moyon, L. G. Delogu and A. Bianco, *Adv Drug Deliv Rev*, 2016, **105**, 163-175.
19. S. Xu, S. Xu, S. Chen, H. Fan, X. Luo, X. Yang, J. Wang, H. Yuan, A. Xu and L. Wu, *J Nanosci Nanotechnol*, 2016, **16**, 4205-4215.

20. D. Murera, S. Malaganahalli, C. Martin, G. Reina, J. D. Fauny, H. Dumortier, E. Vazquez and A. Bianco, *Nanoscale*, 2019, **11**, 10493-10503.
21. M. Orecchioni, V. Bordoni, C. Fuoco, G. Reina, H. Lin, M. Zoccheddu, A. Yilmazer, B. Zavan, G. Cesareni, D. Bedognetti, A. Bianco and L. G. Delogu, *Small*, 2020.
22. M. Orecchioni, D. Bedognetti, L. Newman, C. Fuoco, F. Spada, W. Hendrickx, F. M. Marincola, F. Sgarrella, A. F. Rodrigues, C. Menard-Moyon, G. Cesareni, K. Kostarelos, A. Bianco and L. G. Delogu, *Nat Commun*, 2017, **8**, 1109.
23. G. Reina, A. Ruiz, D. Murera, Y. Nishina and A. Bianco, *ACS Appl Mater Interfaces*, 2019, **11**, 7695-7702.
24. J. Russier, V. Leon, M. Orecchioni, E. Hirata, P. Virdis, C. Fozza, F. Sgarrella, G. Cuniberti, M. Prato, E. Vazquez, A. Bianco and L. G. Delogu, *Angew Chem Int Ed Engl*, 2017, **56**, 3014-3019.
25. S. Gurunathan, M. H. Kang, M. Jeyaraj and J. H. Kim, *Int J Mol Sci*, 2019, **20**.
26. V. Bordoni, G. Reina, M. Orecchioni, G. Furesi, S. Thiele, C. Gardin, B. Zavan, G. Cuniberti, A. Bianco, M. Rauner and L. G. Delogu, *Nanoscale*, 2019, **11**, 19408-19421.
27. Y. Luo, J. Peng, C. Huang and Y. Cao, *Ecotoxicol Environ Saf*, 2020, **199**, 110714.
28. S. P. Mukherjee, O. Bondarenko, P. Kohonen, F. T. Andon, T. Brzicova, I. Gessner, S. Mathur, M. Bottini, P. Calligari, L. Stella, E. Kisin, A. Shvedova, R. Autio, H. Salminen-Mankonen, R. Lahesmaa and B. Fadeel, *Sci Rep*, 2018, **8**, 1115.
29. M. D. Cooper, *Nat Rev Immunol*, 2015, **15**, 191-197.
30. I. A. Vacchi, C. Spinato, J. Raya, A. Bianco and C. Menard-Moyon, *Nanoscale*, 2016, **8**, 13714-13721.
31. M. Hadjidemetriou and K. Kostarelos, *Nat Nanotechnol*, 2017, **12**, 288-290.
32. M. P. Monopoli, D. Walczyk, A. Campbell, G. Elia, I. Lynch, F. B. Bombelli and K. A. Dawson, *J Am Chem Soc*, 2011, **133**, 2525-2534.
33. A. L. Wurster, V. L. Rodgers, M. F. White, T. L. Rothstein and M. J. Grusby, *J Biol Chem*, 2002, **277**, 27169-27175.
34. M. A. Unal, F. Bayrakdar, L. Fusco, O. Besbinar, C. E. Shuck, S. Yalcin, M. T. Erken, A. Ozkul, C. Gurcan, O. Panatli, G. Y. Summak, C. Gokce, M. Orecchioni, A. Gazzi, F. Vitale, J. Somers, E. Demir, S. S. Yildiz, H. Nazir, J. C. Grivel, D. Bedognetti, A. Crisanti, K. C. Akcali, Y. Gogotsi, L. G. Delogu and A. Yilmazer, *Nano Today*, 2021, **38**, 101136.
35. A. D. Amir el, K. L. Davis, M. D. Tadmor, E. F. Simonds, J. H. Levine, S. C. Bendall, D. K. Shenfeld, S. Krishnaswamy, G. P. Nolan and D. Pe'er, *Nat Biotechnol*, 2013, **31**, 545-552.
36. C. S. Bonder, J. J. Finlay-Jones and P. H. Hart, *Immunology*, 1999, **96**, 529-536.
37. I. Voskoboinik, J. C. Whisstock and J. A. Trapani, *Nat Rev Immunol*, 2015, **15**, 388-400.
38. J. M. Kelly, N. J. Waterhouse, E. Cretney, K. A. Browne, S. Ellis, J. A. Trapani and M. J. Smyth, *J Biol Chem*, 2004, **279**, 22236-22242.
39. M. Hagn, K. Sontheimer, K. Dahlke, S. Brueggemann, C. Kaltenmeier, T. Beyer, S. Hofmann, O. Lunov, T. F. Barth, D. Fabricius, K. Tron, G. U. Nienhaus, T. Simmet, H. Schrezenmeier and B. Jahrsdorfer, *Immunol Cell Biol*, 2012, **90**, 457-467.
40. M. J. Leandro, *Arthritis Res Ther*, 2013, **15 Suppl 1**, S3.
41. D. S. Jones, *Pharm Res*, 1995, **12**, 2057-2059.
42. N. C. Sahoo, K. V. Rao and K. Natarajan, *Scand J Immunol*, 2002, **55**, 577-584.
43. M. J. McCarron, P. W. Park and D. R. Fooksman, *Blood*, 2017, **129**, 2749-2759.
44. J. Roelands, D. Bedognetti, J. Decock, E. Wang, W. Hendrickx, *Emerg Top Life Sci*, 2017, **1**, 429–445.
45. M. Dorner, S. Brandt, M. Tinguely, F. Zucol, J. P. Bourquin, L. Zauner, C. Berger, M. Bernasconi, R. F. Speck and D. Nadal, *Immunology*, 2009, **128**, 573-579.
46. E. P. Browne, *Immunology*, 2012, **136**, 370-379.
47. A. Kamburov, U. Stelzl, H. Lehrach and R. Herwig, *Nucleic Acids Res*, 2013, **41**, D793-800.

48. S. P. Mukherjee, N. Lozano, M. Kucki, A. E. Del Rio-Castillo, L. Newman, E. Vazquez, K. Kostarelos, P. Wick and B. Fadeel, *PLoS One*, 2016, **11**, e0166816.
49. S. C. Bendall, E. F. Simonds, P. Qiu, A. D. Amir el, P. O. Krutzik, R. Finck, R. V. Bruggner, R. Melamed, A. Trejo, O. I. Ornatsky, R. S. Balderas, S. K. Plevritis, K. Sachs, D. Pe'er, S. D. Tanner and G. P. Nolan, *Science*, 2011, **332**, 687-696.
50. P. Du, W. A. Kibbe and S. M. Lin, *Bioinformatics*, 2008, **24**, 1547-1548.
51. M. E. Ritchie, B. Phipson, D. Wu, Y. Hu, C. W. Law, W. Shi and G. K. Smyth, *Nucleic Acids Res*, 2015, **43**, e47.
52. C. Martin, *Encyclopedia of Systems Biology*, 2013.
53. R. Herwig, C. Hardt, M. Lienhard and A. Kamburov, *Nat Protoc*, 2016, **11**, 1889-1907.
54. M. Kanehisa, M. Furumichi, M. Tanabe, Y. Sato and K. Morishima, *Nucleic Acids Res*, 2017, **45**, D353-D361.
55. D. Nishimura, *Biotech Software & Internet Report*, 2001, **2**, 117–120.
56. A. Fabregat, Konstantinos Sidiropoulos, Guilherme Viteri, Oscar Forner, Pablo Marin-Garcia, Vicente Arnau, Peter D'Eustachio, Lincoln Stein, Henning Hermjakob, *BMC Bioinformatics*, 2017, **18**, 142.
57. D. N. Slenter, M. Kutmon, K. Hanspers, A. Riutta, J. Windsor, N. Nunes, J. Melius, E. Cirillo, S. L. Coort, D. Digles, F. Ehrhart, P. Giesbertz, M. Kalafati, M. Martens, R. Miller, K. Nishida, L. Rieswijk, A. Waagmeester, L. M. T. Eijssen, C. T. Evelo, A. R. Pico and E. L. Willighagen, *Nucleic Acids Res*, 2018, **46**, D661-D667.
58. W. Huang da, B. T. Sherman and R. A. Lempicki, *Nat Protoc*, 2009, **4**, 44-57.
59. V. D. Blondel, Jean-Loup Guillaume, Renaud Lambiotte, Etienne Lefebvre, *Journal of Statistical Mechanics: Theory and Experiment* 2008, **10**, P10008.

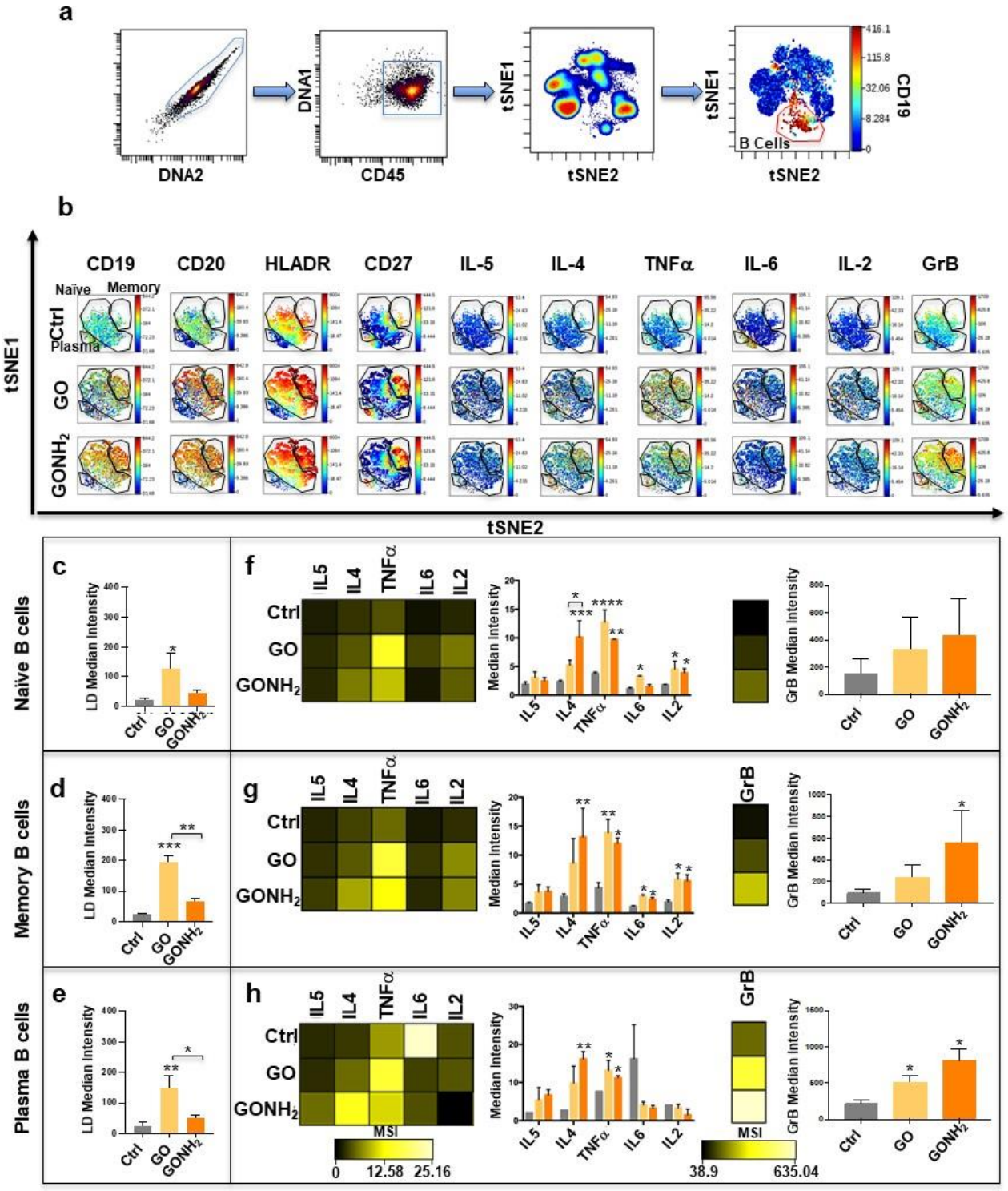

Figure 1. Analysis of the B cell response after GO and $GONH_2$ treatment using single-cell mass cytometry. **a**) Plots showing the use of viSNE to obtain a comprehensive single-cell view and to distinguish the CD45+ PBMC subpopulations. **b**) The tSNE Plots showing the viSNE deconvoluted B cell subpopulations in the GO and $GONH_2$ treated cells. All plots showing the markers and cytokines analyzed are reported**.** **c-e**) Cell viability analysis using cisplatin (LD) median intensity\

on CyTOF of B cells sub populations**. f-g**) Representative Heat map and bar graphs of median marker expression ratio for gated B cell subpopulations. IL5, IL4, IL6, IL2, TNFα and Granzyme b median signal intensity (MSI) is reported. All the experiments were performed in triplicate and shown as means±SD. *p<0.05; **p<0.01, ***p<0.001 by one-way ANOVA with Bonferroni post tests and Tukey's multiple comparisons test.

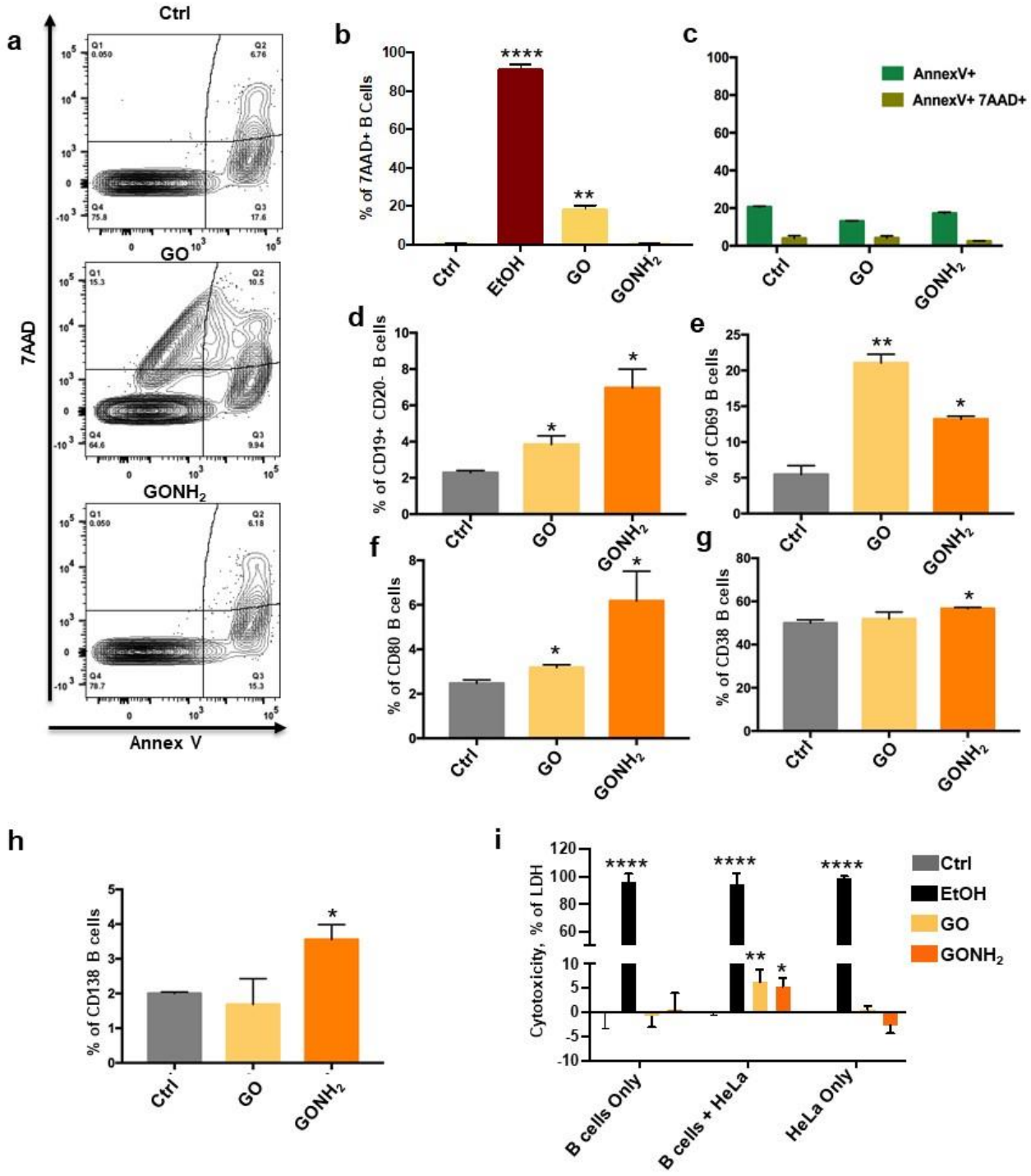

Figure 2. B cell activation assays. Purified B cells from PBMCs were incubated with GO and $GONH_2$ at fixed dose (50 μg/mL) or left untreated for 24h. **a**-**c**) Dot plots and histograms of necrotic and apoptotic cell detection assessed using **b**) 7AAD and **c**) AnnexV markers by flow cytometry. Ethanol 70% was used as positive control. **d**) Histograms on the CD19+ and CD20- B cells population after GO and $GONH_2$ treatment. Percentage of **e**) CD69, **f**) CD80, **g**) CD38, and **h**) CD138, cell surface markers expression on CD19+ B cells were analyzed by flow cytometry.

i) Killing assay of B cells cocultured with Hela cells and treated with GO and $GONH_2$ at fixed dose (50 μg/mL) or left untreated determined by LDH assay. All the experiments were performed in

triplicate and shown as means ±SD. *p<0.05; **p<0.01, ***p<0.001 by one-way ANOVA with Bonferroni post tests and Tukey's multiple comparisons test.

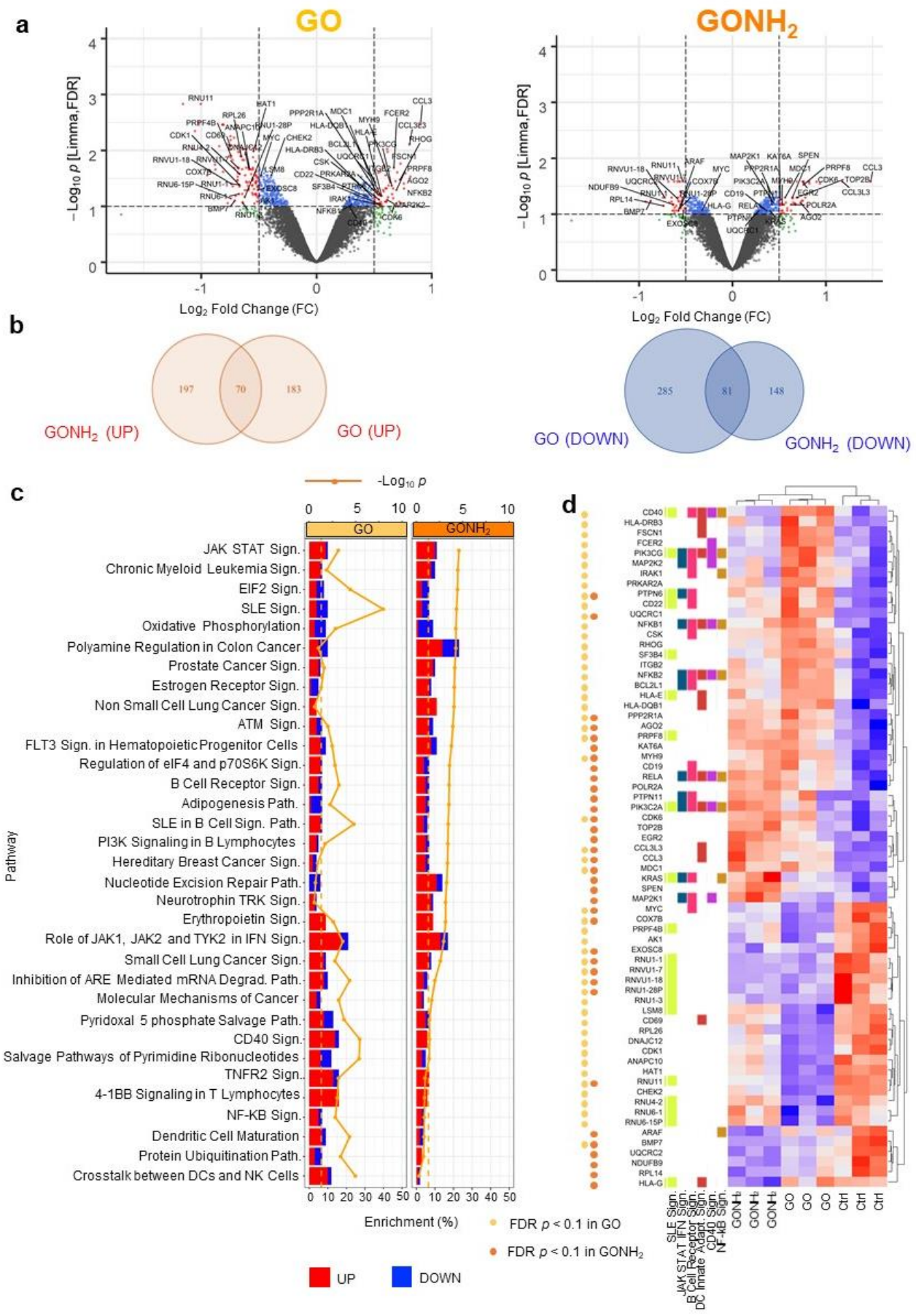

Figure 3. Differentially expressed genes in GO and GONH₂ treated B cells. a) Volcano plots of

differentially expressed genes (DEG; $p < 0.005$, FDR < 0.1, limma model) for $GONH_2$ vs Control and GO Vs Control. When a gene is differentially expressed in one comparison (i.e., GO vs Ctrl) it is also represented in the other comparison (i.e., GONH2 vs Ctrl) independently of the *p* value. **b**) Venn diagrams of DEGs in GO and $GONH_2$. **c**) Top 20 differentially IPA canonical pathways modulated by each material, resulting in 33 unique pathways. When a pathway is differentially expressed in one comparison (ie, GO vs Ctrl) it is also represented in the other comparison ($GONH_2$ vs Ctrl), independently of the *p* value. **d**) Heatmap of representative DEGs. In this heatmap, similar canonical pathways are aggregated (see Table S2). Genes labeled in panel a) and d) include the top modulated transcripts and/or the ones that are included in the top 20 modulated pathways.

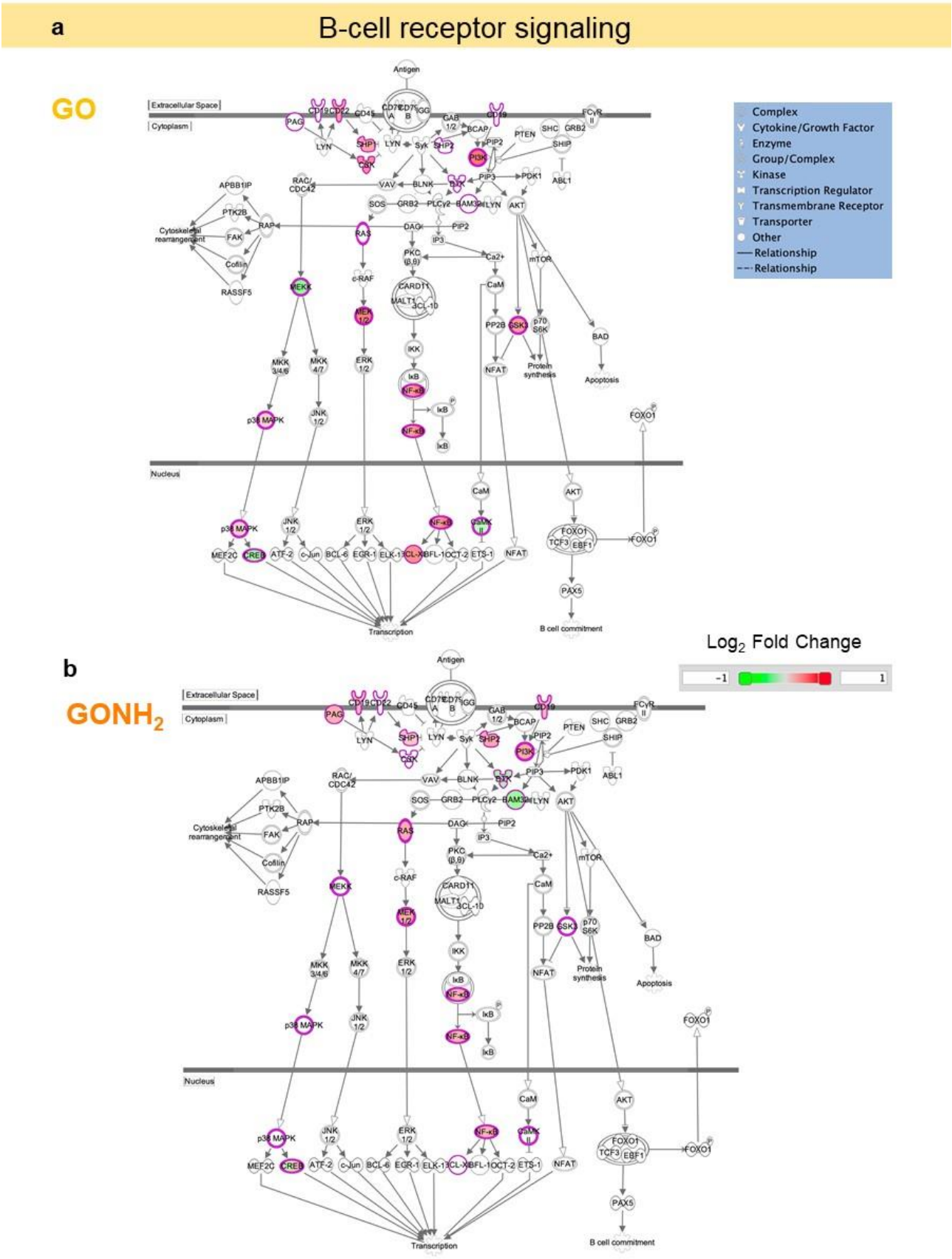

Figure 4. B-cell receptor signaling pathways in GO and $GONH_2$ treated B cells.

Representation of B-cell receptor IPA canonical pathway for GO vs Control (**a**) and $GONH_2$ Vs Control (**b**). Differentially expressed genes (DEG; $p < 0.005$, FDR < 0.1, limma model) are colored

according to Log_2 Fold Change. Purple border indicates that the gene is differentially expressed in either GO vs Control or $GONH_2$ vs Control comparison.

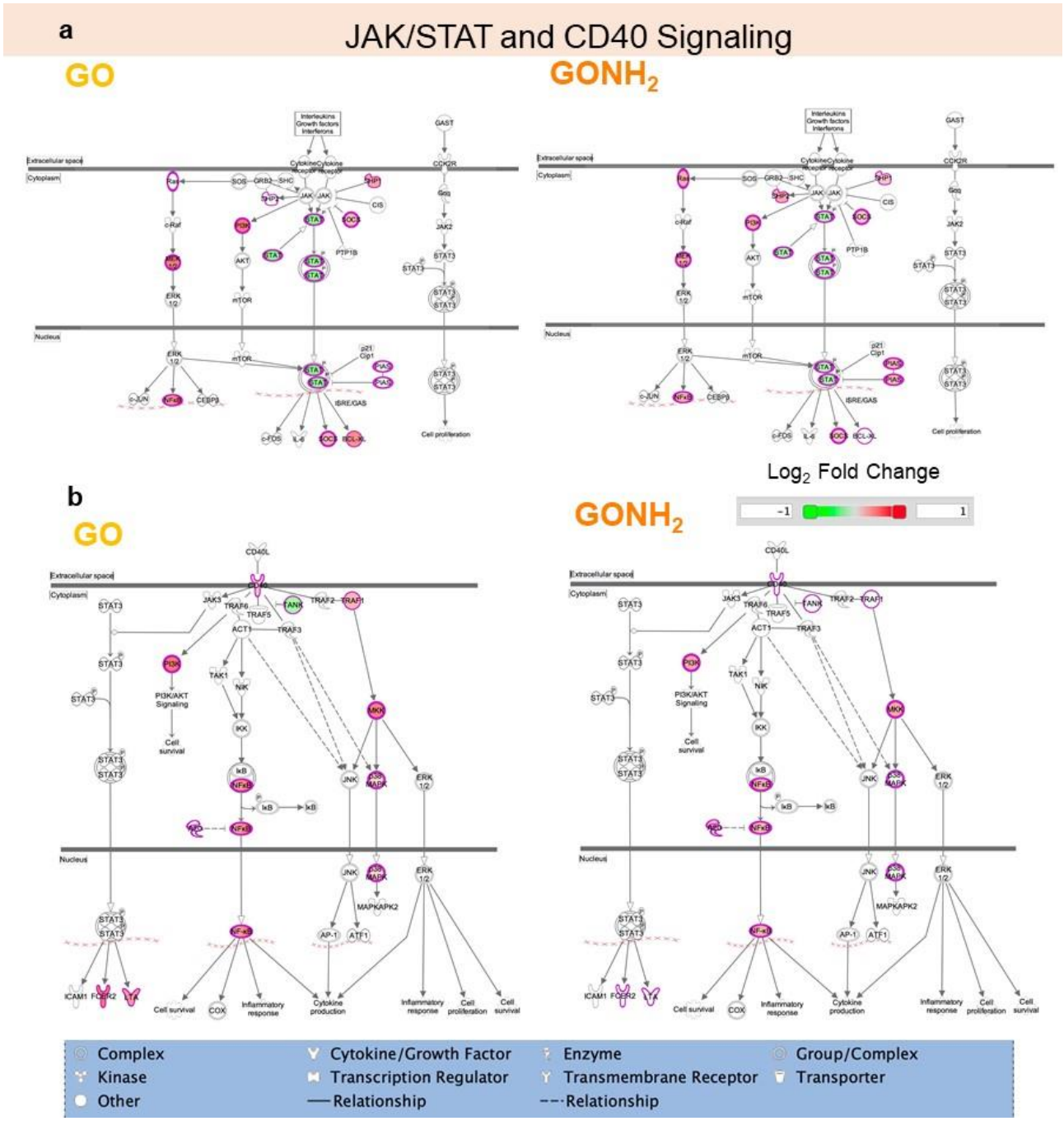

Figure 5. JAK/STAT and CD40 signaling pathways in GO or GONH2-treated B cells.

Representation JAK/STAT (**a**) and CD40 signaling (**b**) IPA canonical pathway for GO vs Control and $GONH_2$ Vs Control. Differentially expressed genes (DEG; $p < 0.005$, FDR < 0.1, limma model) are colored according to Log_2 Fold Change. Purple border indicates that the gene is differentially expressed in either GO vs Control or $GONH_2$ vs Control comparison.

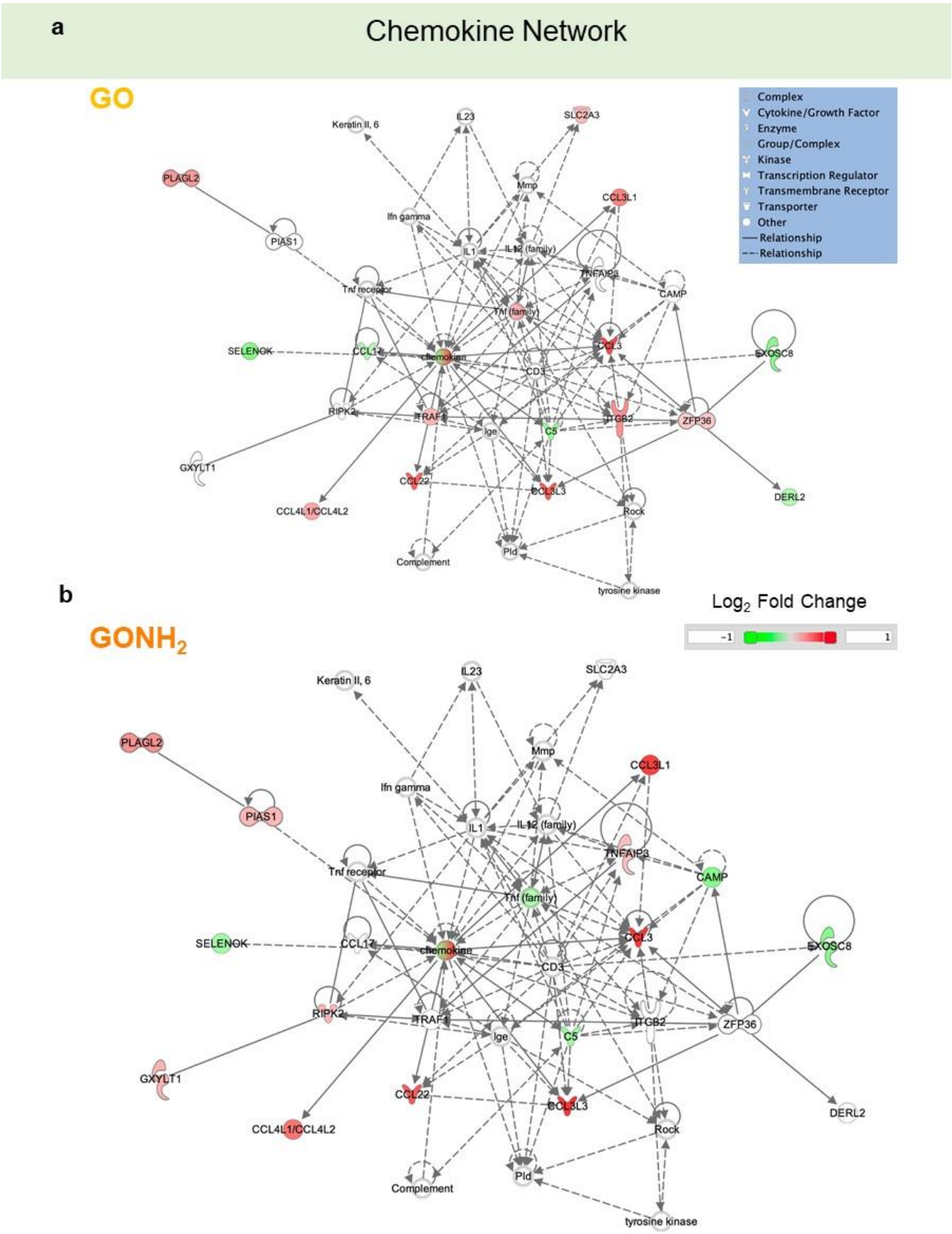

Figure 6. Chemokine network in GO and $GONH_2$ treated B cells. Chemokine network obtained using the list of differentially expressed genes (DEG; $p < 0.005$, FDR < 0.1, limma model) in ether GO (**a**) vs Control or $GONH_2$ Vs Control (**b**). Differentially expressed genes (DEG; $p < 0.005$, FDR < 0.1, limma model) are colored according to Log_2 Fold Change.